ELASTO-PLASTIC DEFORMATION OF HOSTUN SAND DURING CYCLIC LOADING IN TRIAXIAL TEST

Eqramul Hoque

Department of Civil Engineering, Bangladesh University of Engineering and Technology, Dhaka – 1000, Bangladesh, INDIA

ABSTRACT

Cyclic triaxial tests were performed on dry air-pluviated solid cylindrical (7 cm diameter and 15 cm high) specimens of Hostun sand (French sand). Both axial and radial strains were measured locally by using, respectively, a pair of Local Deformation Transducers (LDTs) and three pairs of gap sensors. An isotropically consolidated specimen (at 78.4 kPa) was subjected to cyclic prestraining (CP) with a large number of relatively large amplitude axial-stress cycles. Elastic Young's modulus E^e defined for an axial strain increment less than 0.002% was evaluated at various stress-states along the CP stress path. The effects of CP were investigated on elastic and plastic deformation characteristics along the CP stress path. Elastic parameters were changed slightly due to CP although the overall elastic deformations along the CP stress path were more stable than the plastic deformation characteristics. The plastic deformation component was drastically affected by CP. As a result, the stress-dilatancy relation was changed in a complicated manner.

Keywords: *Triaxial, Local-strains, Cyclic, Elasticity, Plasticity, Prestraining*

INTRODUCTION

A soil mass upon which a structure is founded often experiences cyclic loading caused by fluctuations in loading intensity. For instance, in the case of wave loading on offshore structures, traffic loading on pavements and heavy machine vibrations on foundations the number of cyclic loading is very large although the magnitude of the non-constant component of loading is relatively small. The effects of a series of small seismic loading may also be included in this category. Cyclic loading should, therefore, be rationally accounted for whenever it is likely to improve safety and/or efficiency in design purpose. Often, engineering judgment is required to decide whether, and to what degree, the effects of cyclic loading phenomena ought to be accounted for.

Precise separation of elastic and plastic components of deformation is essential for proper elasto-plastic modeling of sand deformation subjected to a wide variety of strain history [1-2]. In this study, this was attempted by measuring elastic strain increment components frequently during shearing. The importance of the above was investigated by comparing the elasto-plastic deformation characteristics of a prestrained specimen with those of a virgin one. Effects of cyclic prestraining (CP) on the deformation of soil is very important also for structures subjected to heavy traffic, seismic activity, machine vibration, and other dynamic loading such as off-shore structures. A large number of loading cycles (of the order of single amplitude axial strain $(\varepsilon_a)_{SA}$=0.02~0.1%) on dry sand has been observed to increase the elastic limit strain and tangent stiffness both in cyclic and monotonic loadings and to decrease significantly damping at relatively large strain levels (say, $(\varepsilon_a)_{SA} \geq 0.01\%$), with relatively smaller effects on the elastic Young's modulus (E^e) [3]. Therefore, the deformation characteristics of a prestrained specimen differ noticeably from that of a virgin one not because of changes in elasticity but because of large changes in plasticity including dilatancy characteristics. Modeling of such a prestrained specimen should, therefore, require proper characterisation of those aspects. Described herein are the effects of CP on elastic and plastic deformation properties in the light of the results from a comprehensive series of triaxial tests.

THE TESTING SYSTEM

The triaxial apparatus used in this study is shown schematically in Figure 1. A solid, cylindrical specimen of 7.5 cm diameter and 15 cm high was tested. Unlike many other conventional triaxial systems, it includes facilities for a) measurements of axial load by using a sensitive and rigid load cell installed within the triaxial cell to eliminate the effects of piston friction, b) automated anisotropic consolidation by controlling axial and radial stresses independently, c) bedding-error-free 'on-sample' direct measurements of axial deformation by using local deformation transducers (LDTs) [4], and d) local measurements of radial deformations of dry specimen by using 3 pairs of proximity transducers mounted on a system of attachment.

One proximity transducer and one dial gage were also used to measure the displacements of the loading cap and the loading piston, respectively. The external strains obtained from the above may include large effects of bedding error. Radial strains were measured at three heights (2.5-, 7.5- and 12.5-cm above from the bottom) of each specimen assuming that radial strain distribution could be less uniform in the vertical direction compared with axial strain distribution. Two sets of proximeters, each set consisting of three, were mounted on a pair of two-direction micrometer tables so that they can be effectively moved along the vertical and horizontal directions at any stage of test if required; horizontal movement/shifting is often required when repeated loading test is performed, since such a test usually brings about large plastic deformations.

Tests were performed by using a stress-controlled loading system [5]. From the functional point of view, the system has two basic components: a static pressure unit and a cyclic pressure unit, both being fed into from a house pressure unit. The house pressure unit consists of (a) an air compressor, which supplies high air pressure; (b) a regulator, which, based on the maximum pressure, provides constant house pressure

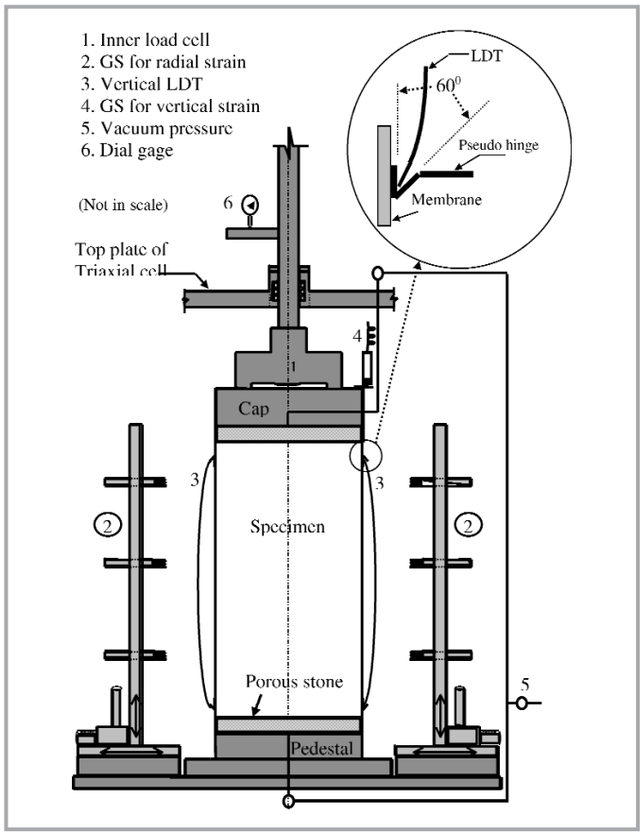

Figure. 1: Triaxial testing system

from the air-compressor; and (c) an accumulator and filter tank unit, which filters and then accumulates supplied air. The static pressure unit, fed by a high pressure line from the accumulator, supplies static pressure via a regulator to the lower chamber of a double-acting Bellofram cylinder. On the other hand, cyclic pressure is controlled by an electro-pneumatic (E-P) transducer through its two inlets. One inlet is connected to the high pressure line from the accumulator. The other receives driving signals for cyclic loading from a control unit. The control unit could be either a software-guided micro-computer or an auto-function generator. Both control units were used in the study. The E-P transducer receives continuous signals, depending on the amplitude and frequency of a cyclic loading (CL) test, from the function generator or computer; it converts the commanding signals into an equivalent pressure through maintaining a static equilibrium on the torque bar seated inside the E-P transducer. Finally, the equivalent pressure after having been amplified in volume by using another regulator (booster) is conveyed to the upper chamber of the Bellofram cylinder. A specimen is directly connected to the Bellofram cylinder through a loading piston. Any change in pressure, static or cyclic, in the Bellofram cylinder results in the corresponding change in the axial stress of the specimen. The confining stress was applied by partial vacuum. Using a 12-bit 16 channel analogue-to-digital converter card, the data acquired by using the transducers is fed into a 16-bit micro-computer.

TEST PROGRAM AND PROCEDURE

The tests were performed on specimens of Hostun sand (collected from France) at dry state. Hostun sand is a fine-grained, quartz-dominant and sub-angular (grain shape) sand. The physical properties of the sand are: D_{10}= 0.17 mm, D_{50}= 0.31 mm, U_C = 1.94, G_S = 2.65, e_{max} = 0.95 and e_{min} = 0.55. A cylindrical specimen (7.5 cm diameter and 15 cm high) was reconstituted by raining air-dried sand particles through air into a split mold. Regular ends (i.e., non-lubricated ends using porous stones) were used at both ends of the specimen. A partial vacuum of 10 kPa was applied to a specimen which was completely enclosed within a rubber membrane before the mold was dissembled. A freestanding specimen was then consolidated isotropically to a pressure σ_c (= 78.4 kPa for all specimens in this study), at which the specimen dimensions were measured before any instrumentation. Cyclic loading tests were then performed symmetrically about a neutral axial stress state.

Test program on a given specimen consisted of CL tests at various amplitudes, which was repeated at different instants of testing to investigate the effects of CP on E^e, elastic and plastic deformation characteristics along the CP stress path. Tests were performed on two specimens HOSTN3 and HOSTN5 with void ratio e, respectively, 0.72 and 0.81 being measured at σ_c = 78.4 kPa.

Elastic Young's modulus (E^e) was evaluated by applying very small cyclic axial load for which the single-amplitude axial strain, $(\varepsilon_a)_{SA}$, was kept within 0.002%. The Young's modulus of a specimen of clean sand evaluated at this strain level is observed to be independent of the type of loading (cyclic or monotonic), rate of shearing (static or dynamic), load-history and the degree of over-consolidation as long as the initial fabric remains essentially unchanged [6-8]. This feature has been validated particularly by the fact that a Young's modulus E^e value thus obtained is essentially similar to that obtained by measuring body wave velocities. So, this value can be considered to be the maximum Young's modulus which a soil element can exhibit in its current state.

Cyclic loading, including CP (i.e., the application of a large number of relatively large amplitude stress cycles along a fixed path), was applied symmetrically about either an isotropic or an anisotropic stress state. Note that in both cases, the radial stress σ_r was 78.4 kPa. The loading frequency (f) for CP was in the range of 0.1 to 0.5 Hz, while it was 0.1 Hz in the CL tests performed for evaluating soil parameters. The latter frequency (i.e., f = 0.1 Hz) was employed to assist a micro-computer to sample a sufficient number of data-per-cycle for analytical purposes. A prescribed number of cyclic loading was applied in CP with a fixed axial-stress amplitude (CP_{str}) during which the value of $(\varepsilon_a)_{SA}$ was changed drastically. Typical relationships between axial stress σ_a , axial strain ε_a and radial strain ε_r are shown in Figure 2. The relationships are plotted for the virgin cycle (i.e., cycle 1), the 2nd, 200th and 25,000th cycles. During CP with CP_{str} on a given specimen (Figure 2), the value of $(\varepsilon_a)_{SA}$ was not a constant value; rather it decreased with the number of loading cycles.

RESULTS AND DISCUSSIONS

Axial strains measured by gap sensor usually include system compliance error [2, 7] and so was the case in the present study. The axial strains ε_a measured by two vertical LDTs (Figure 1), on averaging, are shown in Figure 2 and the following figures if not otherwise specified. In this and the following figures, if not specified otherwise, the axial stress and/or the stiffness (i.e., E^e) are normalised by dividing it with

pressure P_a (= 98 kPa). The ε_a and ε_r axes for the prestrained specimen (i.e., after CP) were shifted arbitrarily. The actual values of strains (ε_a and ε_r) at the bottom ends of the curves for the prestrained specimen (denoted as S_p) can be seen from Figure 3, in which the translation of strain axes with the number of loading cycles at the reference stress state $\sigma_a = \sigma_r =$ 78.4 kPa are shown in semi-logarithmic plot. In the figure, the volumetric strain ε_{vol}, defined as $\varepsilon_a+2\varepsilon_r$, was also shown. It can be seen that translation was maximum in the first cycle; the translation was maximum in the direction of major principal strain (i.e., ε_a); the ε_a axis was translated almost linearly after the first cycle in the semi-logarithmic scale, while it was almost constant in ε_r axis; consequently, ε_{vol} axis was translated at a smaller rate. Even after the application of a large number of prestraining cycles, the translation of strain axis in the major principal direction did not cease completely.

Elastic Young's modulus E^e was evaluated at various stress states along the CP stress path both before and after CP. Before CP, it was measured during the 3rd cycle. Note that the elastic parameters (E^e and the elastic Poisson's ratio ν) were evaluated by applying very small amplitude cyclic loads in which the single amplitude axial strain was less than 0.002%. Figure 4 shows the relationships between $E^e/f(e)$ and the axial stress σ_a

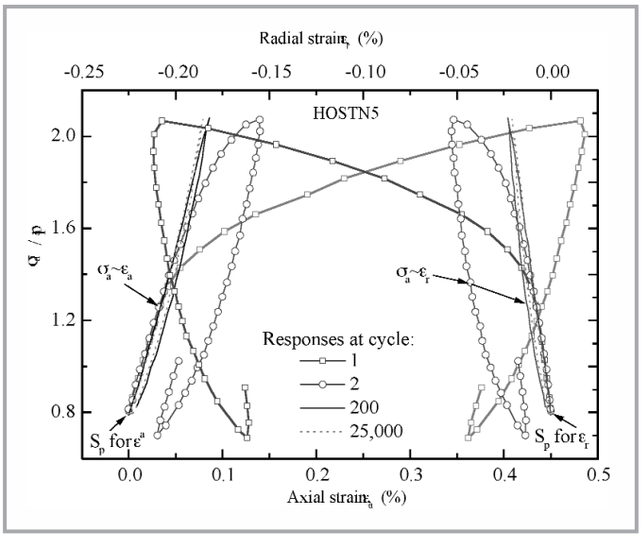

Figure 2: *σ_{a}~ε_{a} and σ_{a}~ε_{r} relationships of large CL tests at virgin state*

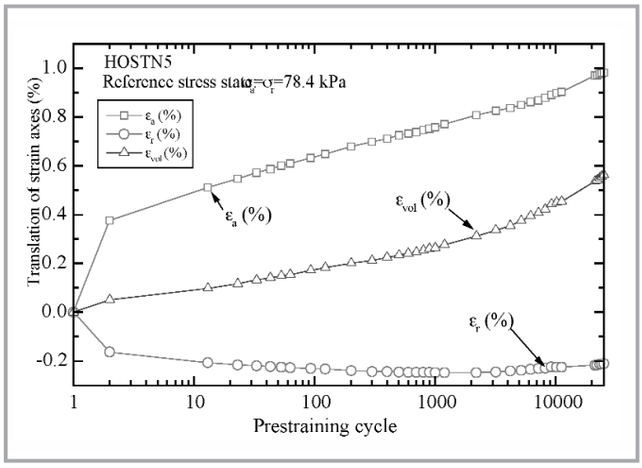

Figure 3: *Translation of sttrain axes with the number of loading cycle during CP*

in full logarithmic scale obtained from HOSTN5 specimen. The E^e value was normalised by dividing it with a void ratio function $f(e) = (2.17- e)^2 / (1+e)$ [9] in order to account for the change in void ratio during the course of testing program. However, the change in void ratio was negligible, which needed less than 1% correction in the measured value of E^e. In the same figure, E^e values measured along the isotropic stress path at virgin state (i.e., before CP application) were also plotted for comparison. It can be seen that $E^e/f(e)$ ~ σ_a relationship obtained from isotropic stress path was similar to that obtained along the CP stress path at the virgin state (i.e., before CP). It indicates that E^e measured for axial strain increment increased with the increase in σ_a. That is, the elastic Young's modulus was a function of axial stress in the direction of major principal strain increment. Among many others, [6,10-11] showed a large number of data supporting the above behavior. Accordingly, the above stress-dependency of Young's modulus can be modeled as [10-11]:

$$E^e = E_1 \text{ x } f(e) \text{ x } (\sigma_a / P_a)^m \qquad (1a)$$

On the other hand, the Poisson's ratio ν (i.e., horizontal-to-vertical strain ratio defined for small increment less than 0.002% in the major principal strain direction) measured along the CP stress path can be modeled as:

$$\nu = \nu_0 \text{ x } (\sigma_a / \sigma_r)^{m/2} \qquad (1b)$$

In the above equation, various entities used are: $E_1 = E^e$ measured at $\sigma_a =$ 98 kPa when $f(e) = 1.0$ (i.e., for $e = 0.82$); $\nu_0 =$ the average value of Poisson's ratio ν measured at isotropic stress states; $P_a =$ atmospheric pressure and m <1.0, a nonlinear exponent relating σ_a with E^e. The values of elastic parameters E_1 / P_a, ν_0 and m for HOSTN5 specimen evaluated at virgin states were, respectively, 1800, 0.20 and 0.47 and those for HOSTN3 specimen were, respectively, 1964, 0.17 and 0.46. It can also be seen from Figure 4a that the stress-dependency relationship between E^e and σ_a was slightly changed due to CP application. As a result, E^e values decreased at larger stress states while it increased at the lower stress states along the CP stress path. Consequently, both E_1/P_a and m values were noticeably changed (i.e., they became 1536, 0.81 for HOSTN5 and 1900, 0.80 for HOSTN3 specimen) from the respective initial values. However, CP did not bring about any changes on the elastic Poisson's ratio ν (and also ν_0) and its dependency on the stress ratio σ_a / σ_r as modeled by Eq.(1b). The detail of modeling E^e and ν were described in [7,12].

Elastic strains for the whole stress range of CP_{str} were obtained by integrating $d\varepsilon_a^e = d\sigma_a / E^e$ and $d\varepsilon_r^e = - \nu$ x $d\varepsilon_a^e = - \nu$ x $d\sigma_a / E^e$ by using the relations Eq.(1a) and Eq.(1b) together with the respective elastic parameters E_1, m and ν_0. Note that these values were affected by CP. The relationships between σ_a and the elastic axial and radial strains (ε_a^e, ε_r^e) were arbitrarily plotted in Figures 5a and b, respectively, with the origins denoted as S_a and S_p at the bottom end (i.e., at $\sigma_a =$ 78.4 kPa for HOSTN5) of the respective σ_a~ε_a and σ_a~ε_r relation for the range of CP_{str}. A drastic changes in the σ_a~ε_a (Figure 5a) and σ_a~ε_r (Figure 5b) relations were caused by a substantial reduction in the plastic strain components ($\varepsilon_a^p = \varepsilon_a - \varepsilon_a^e$, $\varepsilon_r^p = \varepsilon_r - \varepsilon_r^e$) due to CP, while the σ_a~ε_a^e relation changed

very slightly due to the change in the elastic parameters. The effects of CP application by 25,000 and 65,000 cycles along the same stress path were very similar (Figures 5a and b). Now it can be understood why the stress-strain relations after CP concave upward with a small hysteresis area. It is interesting to note that the $\varepsilon_r^{\ e}$ and σ_a relation happened to be linear. The behavior described above was due to the intrinsic elastic

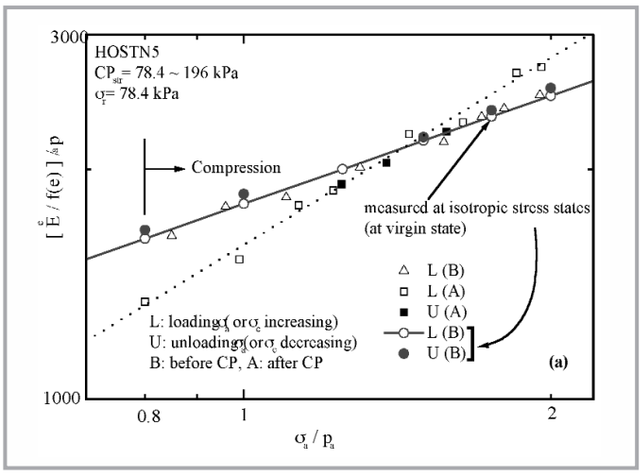

***Figure 4a:** Relationship between* E^e *and* σ_a *of HOSTN5 specimen*

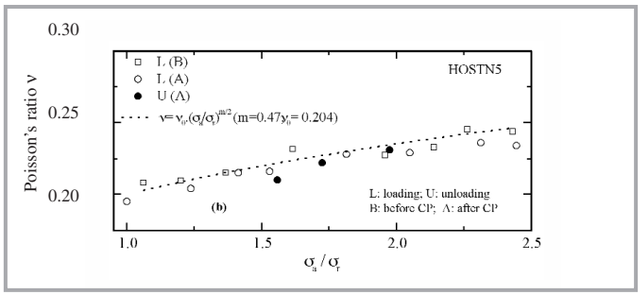

***Figure 4b:** Relationship between* ν *and* σ_a/σ_r *along CP sstress path*

property of sand. That is, according to Eq. 1a, the elastic behavior of a sand is hypo-elastic type [10] and if one estimates the elastic strain component along a fixed stress path, the shape of the resulting elastic-strain and stress curve would be concave upward. Similar shape (i.e. concave upward) of the stress-strain curves (Figures 5a and b) was resulted from after CP application, indicating the dominance of elastic-strain component in total strain.

A considerable decrease in the plastic-to-elastic strain increment ratio occurred due to CP, which can be observed from Figures 6 and 7 for HOSTN3 and HOSTN5 specimen, respectively. The relationship between plastic-to-elastic strain increment ratio in axial direction (r_a) and σ_a , both before and after CP, are shown in Figures 6a and 7a, respectively, for HOSTN3 and HOSTN5 specimen. Similar relationship between plastic-to-elastic strain increment ratio in radial direction (r_r) and σ_a are shown in Figures 6b and 7b, respectively, for HOSTN3 and HOSTN5 specimen. It can be seen from Figures 6 and 7 that before CP, the elastic-to-plastic strain increment ratios (i.e., r_a and r_r) varied widely and nonlinearly with σ_a , whereas after CP, it varied narrowly and more-or-less linearly with σ_a during

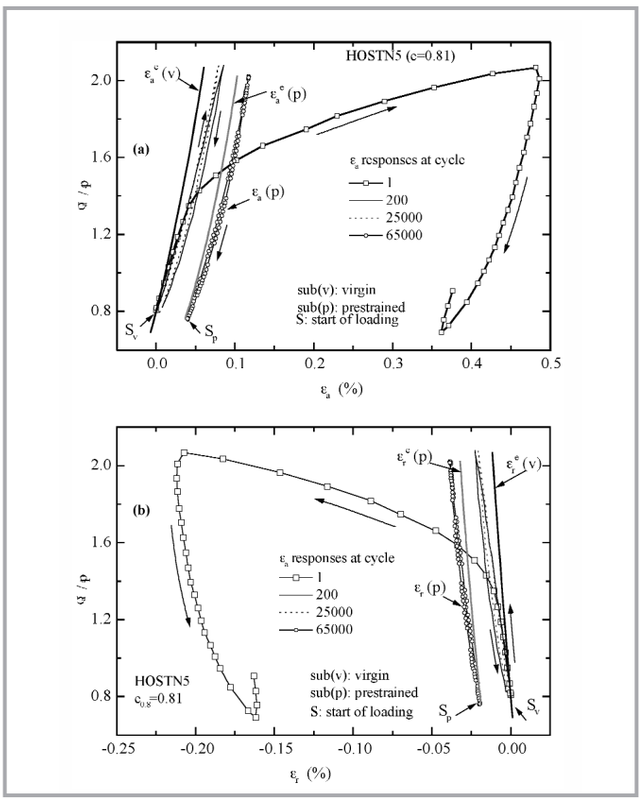

***Figure 5:** (a)* σ_a~ε_a *and (b)* σ_a~ε_r *relationships of virgin and prestrained states in CP stress path*

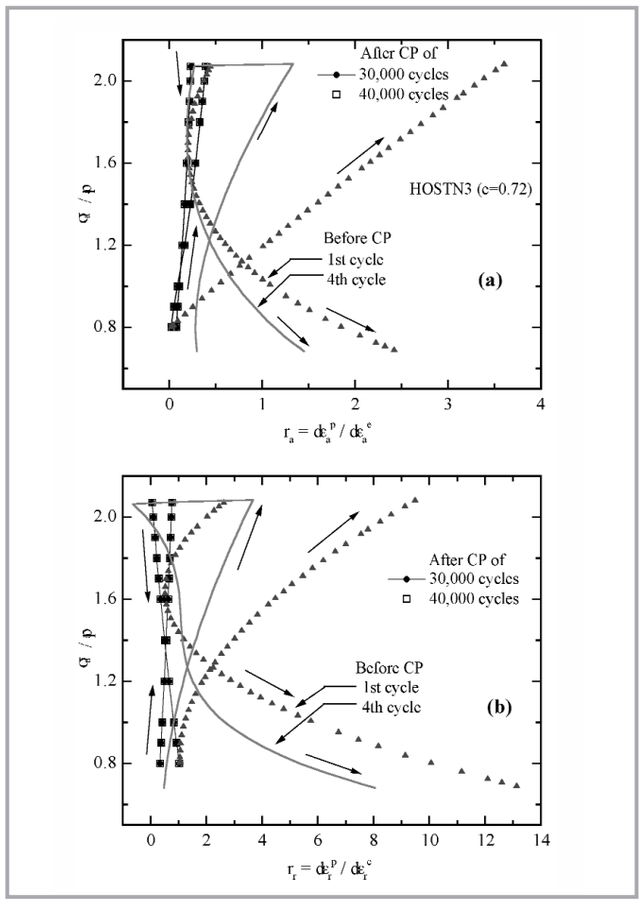

***Figure 6:** (a)* σ_a~ε_a *and (b)* σ_a~ε_r *relationships of virgin and prestrained states in CP stress path*

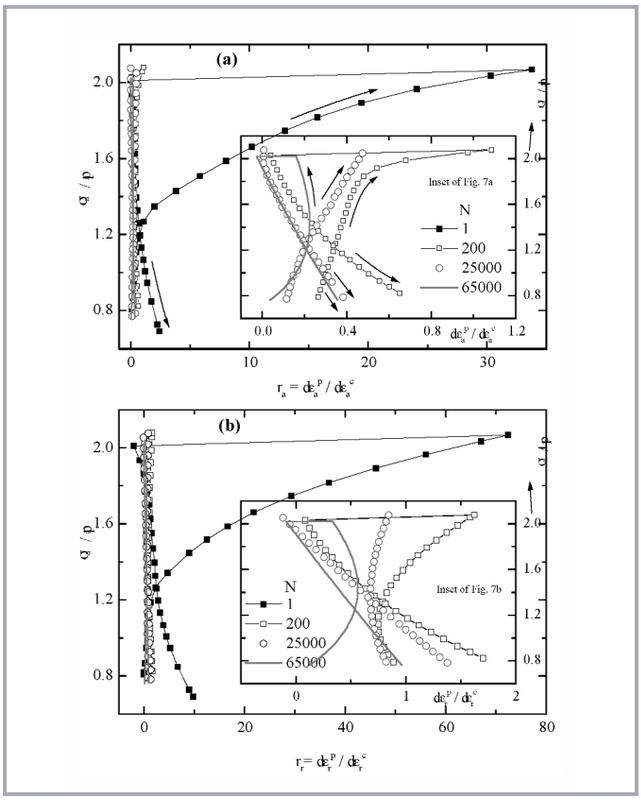

Figure 7: *(a)* σ_a~ε_a *and (b)* σ_a~ε_r *relationships of virgin and prestrained states in CP stress path*

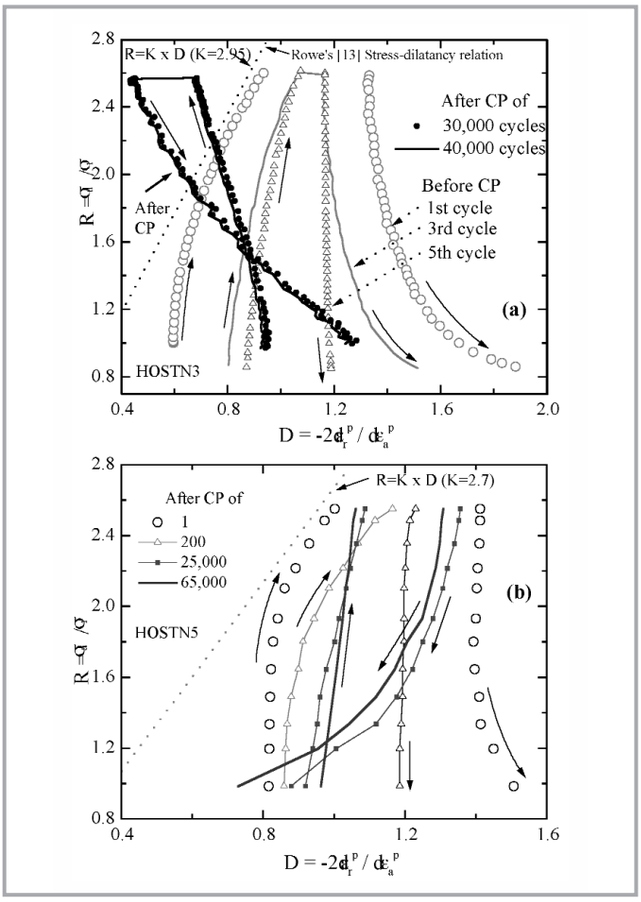

Figure 8: *(a)* σ_a~ε_a *and (b)* σ_a~ε_r *relationships of virgin and prestrained states in CP stress path*

both loading and unloading. For a given specimen (i.e., void ratio) before CP, the r_a values varied in much wider ranges than that occurred in r_r values. On the other hand, at a given stress level, for loose specimen (HOSTN5) the values of r_a and r_r were significantly larger than those of the dense specimen (HOSTN3). However, for both specimens after CP, both r_a and r_r values became narrowly varying within the CP stress path.

It is important to note that the higher values of r_a and r_r before CP application indicate that the deformations at this stage were dominated by the plastic strain components. As the number of prestraining cycle increased, the values of r_a and r_r decreased drastically, indicating the decrease of plastic strain component compared to the elastic strain component. Besides, significant difference was observed between the values of r_a and r_r if one compares the data of the 1st cycle and the 4th cycle (Figures 6a and b). However, after the application of a large number of prestraining cycles in the same stress path, the r_a and r_r values were in the range between 0.5 to 2.0 (Figures 6 and 7). Therefore, the deformation, in no cases, for the whole range of σ_a (CP_{str}) which was applied as CP did not become totally elastic even after the application of a very large number of CP stress cycles. On the other hand, cyclic prestraining by 30,000 and 40,000 cycles did not show any difference for medium dense specimen HOSTN3 (Figures 6a and b), whereas some differences could be observed between the responses after 25,000 and 65,000 cycles in the loose specimen HOSTN5 (Figures 7a and b).

Figures 8a and b show the relationships, respectively, of HOSTN3 and HOSTN5 between the stress ratio ($R = \sigma_a / \sigma_r$) and the dilatancy rate (defined as $D = -2d\varepsilon_r^p / d\varepsilon_a^p$). The relation (i.e., $R \sim D$) during loading at the virgin states followed closely the Rowe's [13] stress-dilatancy relation $R = K \times D$ with K=2.95 for HOSTN3 and K= 2.7 for HOSTN5. But the linear stress-dilatancy relationship (i.e., $R = K \times D$) did not observe in case of unloading, reloading and re-unloading. Before CP, the relations approached to the non-plastic volumetric strain increment condition (i.e., $D = 1.0$) for both loading ($d\sigma_a > 0$) and unloading ($d\sigma_a < 0$). The relations after CP showed a different trend; during loading more contractive behavior (i.e. $D > 1.0$) with the increase in $R = \sigma_a / \sigma_r$, whereas during unloading more dilative behavior (i.e $D < 1.0$) could be observed. This behavior was much more complicated than the behavior predicted by Pradhan and Tatsuoka [14].

Figures 9a and b show the relationships between R and plastic prestrain-to-virgin shear strain increment ratio (*PPVS*) for specimens HOSTN3 and HOSTN5, respectively. *PPVS* decreased significantly for both loading ($\Delta\sigma_a > 0$) and unloading ($\Delta\sigma_a < 0$) with a large discontinuity along *PPVS* axis at the point of stress reversal. With the increase in loading cycle (i.e. CP), the value of *PPVS* for a given σ_a gradually decreased in such a way that the $\sigma_a \sim PPVS$ relation for a particular cycle (during loading or unloading) remained parallel to the similar relation at virgin state.

CONCLUSIONS

Elastic Young's modulus E^e of Hostun sand was axial stress dependent. That is, E^e measured in the axial stress direction by applying very small amplitude cyclic loading was a function of

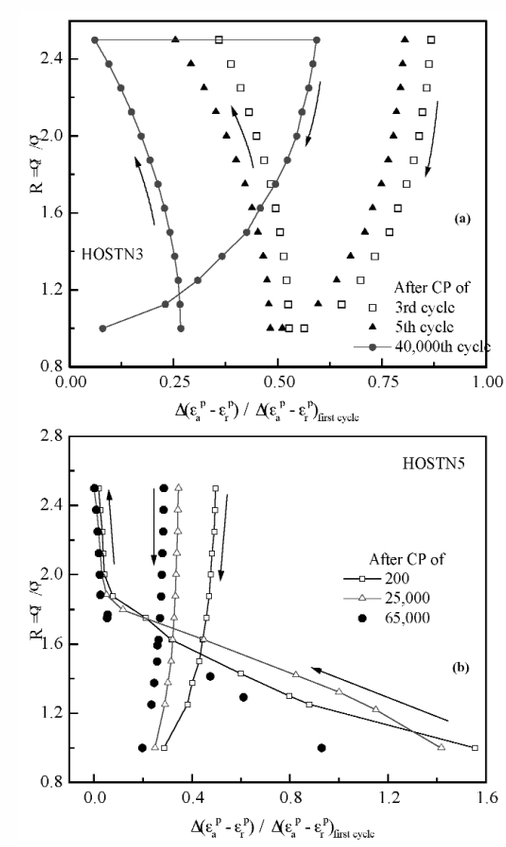

***Figure 9:** (a) σ_a~ε_a and (b) σ_a~ε_r relationships of virgin and prestrained states in CP stress path*

the axial stress (σ_a) only and it increased nonlinearly with the increase in σ_a. Deformation characteristics of the sand during a relatively large amplitude stress cycle were dominated by plastic strain component at virgin state. With the increase of the application of prestraining cycles along the fixed stress path, the plastic strain increment decreased drastically. Therefore, the elastic strain component became equally significant as the plastic strain component. Deformation did not become totally elastic even after the application of a large amount of CP with a relatively large amplitude of axial stress cycle. The elastic deformation characteristics were much more stable compared to plastic deformations, but they also changed slightly due to CP. Therefore, the deformation of sand cannot be modeled precisely by a simple elasto-plastic model having a fixed range of elasto-plastic parameters. The stress-dilatancy relation was changed by cyclic loading in a complicated manner. ■

REFERENCES

[1] J.B. Burland, "Small is beautiful-the stiffness of soils at small strains", *Ninth Laurits Bjerrum Memorial Lecture, Canadian Geotechnical Journal*, Vol. 26, pp. 499-516, 1989.

[2] F. Tatsuoka, S. Teachavorasinskun, J. Dong, Y. Kohata and T. Sato, "Importance of measuring local strains in cyclic triaxial tests on granular materials", *Dynamic Geotech. Testing, ASTM STM 1213*, ASTM, pp. 288-302, 1994.

[3] S. Teachavorasinskun, *Deformation Characteristics of Sands at Small Strains*, Doctoral thesis, The University of Tokyo, 1992.

[4] S. Goto, F. Tatsuoka, S. Shibuya, Y-S. Kim and Y. Sato, "A Simple Gauge for Local Small Strain Measurements in the Laboratory", *Soils and Foundations*, Vol. 31, No. 1, pp. 169-180, 1991.

[5] E. Hoque and F. Tatsuoka, "Triaxial testing-system measuring loading-rate effects during cyclic tests of sand", *Geotechnical Testing Journal*, ASTM, Vol. 27, No. 5, pp. 483-495, Sept. 2004.

[6] M. Jamiolkowski, S. Lerouell and D.C.F. Lo Presti, "Design parameters from theory to practice", *Theme Lecture, Geo-Coast '91*, Yokohama, pp. 877-917, 1991.

[7] E. Hoque, F. Tatsuoka and T. Sato, "Measuring anisotropic elastic properties of sand using a large triaxial specimen", *Geotech. Testing J., ASTM*, Vol. 19, No. 4, pp. 411-420, 1996.

[8] F. Tatsuoka, R.J. Jardine, D. Lo Presti, H. Di Benedetto and T. Kodaka, "Characterizing the pre-failure deformation properties of geomaterials", *Theme Lecture for the Plenary Session No. 1, 14th Int. Conf. On SMFE, Hamburg*, Vol. 2, 1997.

[9] B.O. Hardin and F.E.Jr. Richart, "Elastic wave velocities in granular soils", *Journal of SMFE, ASCE*, Vol. 89, No. SM1, pp. 33-65, 1963.

[10] E. Hoque and F. Tatsuoka, "Anisotropy in elastic deformation of granular materials", *Soils and Foundations*, Tokyo, Vol. 38, No. 1, pp. 163-179, 1998.

[11] K.H.II. Stokoe, J.N.K. Lee and S.H. Lee, "Characterization of soil in calibration chambers with seismic waves", *Proc. Of Int. Symp.on Calibration Chamber Testing*, Clarkson Univ., Potsdam, NewYork, Huang Edition, Elsevier, pp. 363-376, 1991.

[12] G.L. Jiang, F. Tatsuoka, A. Flora and J. Koseki, "Inherent and stress state-induced anisotropy in very small strain stiffness of a sandy gravel", *Geotechnique*, 47-3, pp. 509-521, 1997.

[13] P.W. Rowe, "The Stress-Dilatancy Relation for State Equilibrium of an Assembly of Particles in Contact", *Proc. Royal Society, 269A*, pp. 500-527, 1962.

[14] T.B.S. Pradhan and F. Tatsuoka, "On Stress-Dilatancy Equations on Sand Subjected to Cyclic Loading", *Soils and Foundations*, Vol. 29, No. 1, pp. 65-81, 1989.